catalysts

MDPI

Article

Flame-Made Cu/TiO_2 and $Cu-Pt/TiO_2$ Photocatalysts for Hydrogen Production

Massimo Bernareggi [1], Maria Vittoria Dozzi [1], Luca Giacomo Bettini [2,3], Anna Maria Ferretti [4], Gian Luca Chiarello [1] and Elena Selli [1,3,*]

1 Dipartimento di Chimica, Università degli Studi di Milano, via Golgi 19, 20133 Milano, Italy; massimo.bernareggi@unimi.it (M.B.); mariavittoria.dozzi@unimi.it (M.V.D.); gianluca.chiarello@unimi.it (G.L.C.)
2 Dipartimento di Fisica, Università degli Studi di Milano, via Celoria 16, 20133 Milano, Italy; lucagiacomo.bettini@unimi.it
3 CIMAINA, Università degli Studi di Milano, via Celoria 16, 20133 Milano, Italy
4 ISTM-CNR Lab Nanotechnology, Via Fantoli 16/15, 20138 Milano, Italy; anna.ferretti@istm.cnr.it
* Correspondence: elena.selli@unimi.it; Tel.: +39-02-503-14237

Academic Editor: Bunsho Ohtani
Received: 8 September 2017; Accepted: 11 October 2017; Published: 13 October 2017

Abstract: The effect of Cu or Cu-Pt nanoparticles in TiO_2 photocatalysts prepared by flame spray pyrolysis in one step was investigated in hydrogen production from methanol photo-steam reforming. Two series of titanium dioxide photocatalysts were prepared, containing either (i) Cu nanoparticles (0.05–0.5 wt%) or (ii) both Cu (0 to 0.5 wt%) and Pt (0.5 wt%) nanoparticles. In addition, three photocatalysts obtained either by grafting copper and/or by depositing platinum by wet methods on flame-made TiO_2 were also investigated. High hydrogen production rates were attained with copper-containing photocatalysts, though their photoactivity decreased with increasing Cu loading, whereas the photocatalysts containing both Cu and Pt nanoparticles exhibit a bell-shaped photoactivity trend with increasing copper content, the highest hydrogen production rate being attained with the photocatalyst containing 0.05 wt% Cu.

Keywords: photocatalysis; flame-spray pyrolysis; TiO_2 modification; Cu and Pt nanoparticles; photocatalytic hydrogen production; methanol photo-steam reforming

1. Introduction

The continued use of fossil fuels led to an increased greenhouse effect; thus, cleaner and renewable energy sources are urgently required. Hydrogen is considered the main alternative to fossil fuels and technologies based on hydrogen exploitation as an energy vector are already mature, such as fuel cells or internal hydrogen combustion engines [1,2]. Photocatalysis can provide a straightforward route to hydrogen production from water solutions, possibly converting solar light into chemical energy in the form of H-H bond.

Many photocatalysts have been proposed and tested in recent years, for both thermodynamically up-hill (e.g., hydrogen production from aqueous solutions) and down-hill reactions (photodegradation of organic pollutants), but titanium dioxide still remains the most widely investigated one, due to its advantageous physical and chemical properties [3,4]. One of its main drawbacks consists in the fast recombination of photoproduced electron-hole couples. This drawback can be overcome by modifying TiO_2 with noble metal (Au, Ag, Pd, Pt) nanoparticles (NPs), which improve the separation of photoproduced charge carriers and, thus, the quantum efficiency of photocatalytic processes [5]. Furthermore, the rate of photocatalytic hydrogen production from water is largely increased by performing the reaction in the presence of organic compounds which scavenge the holes

photoproduced in the semiconductor valence band (VB) more efficiently than water, making the reaction irreversible [6–11].

Aiming at increasing the photoactivity of titanium dioxide by modification with non-noble metals (e.g., Ni, Cu, Co), thus reducing the photocatalyst costs, Irie et al. [12] deposited copper on titanium dioxide powders by grafting. This led to successful visible light activation of the so obtained photocatalysts both in oxidation reactions (photodegradation of organic pollutants, e.g., 2-propanol) in the presence of O_2 and in hydrogen production from water solutions under anaerobic conditions [13]. In fact, Cu^{2+} ions are able (i) to accept electrons from the conduction band (CB) of TiO_2, since the redox potential of the Cu^{2+}/Cu^{+} couple is more positive than the CB edge of TiO_2; and (ii) to accept photoexcited electrons directly from the VB of TiO_2, also under visible light irradiation. Both these electron transfer paths contribute to increase the separation of photoproduced charge carriers, with a consequent photoactivity improvement [10].

To further increase the photoactivity of TiO_2, modification of the oxide surface by non-noble metals, such as copper or nickel, has been coupled with noble metal (i.e., Au, Pt, Ag) NPs deposition, attaining remarkable improvement in terms of photocatalytic hydrogen production rates and efficiency in solar light exploitation [14–18]. In this context, synergistic effects in photoactivity have been demonstrated in the case of copper-platinum co-modified TiO_2 when small amounts of Cu were deposited together with Pt NPs, under both aerobic [19] and anaerobic conditions [20,21]. A strong synergistic effect between copper and platinum NPs deposited over TiO_2 has been recently demonstrated in hydrogen production by methanol photo-steam reforming by our research group [22]. The NPs of the two metals were deposited on commercial titanium dioxide in subsequent steps, i.e., Cu(II) was pre-grafted on the oxide surface, followed by Pt NP deposition and chemical reduction.

In the present work, we investigate another, potentially less time consuming, synthetic route to produce Cu and Cu-Pt co-modified TiO_2 photocatalysts in one step, i.e., flame spray pyrolysis (FSP), and report on the structural characterization of the so obtained materials in relation to their photoactivity in methanol photo-steam reforming. The FSP technique proved to be an effective method to synthesize TiO_2 photocatalyst powders containing noble metal NPs with high anatase content and crystallinity, high surface area and excellent metal dispersion [23–26], which are particularly suitable for photocatalytic hydrogen production from water solutions. In addition, three photocatalysts obtained either by grafting copper and/or by depositing platinum by wet methods on FSP-made TiO_2 were also investigated for comparison.

2. Results and Discussion

2.1. Photocatalyst Characterization

2.1.1. XRPD and BET Analyses

As shown in Figure 1, the X-ray powder diffraction (XRPD) pattern of pure titanium dioxide FP-T showed a biphasic crystalline composition (89% anatase, 11% rutile) with no evidence of brookite reflections; the mean crystallite size of the anatase phase was 14 nm (Table 1). The XRPD analysis of both FP-(X)Cu-T and FP-(X)Cu/Pt-T series indicate that the anatase crystallite mean size appear to increase with increasing copper content, as well as the rutile/anatase ratio, a phenomenon which has already been observed in previous studies [27]. Nevertheless, no reflections due to the metals or to copper oxides were detected, suggesting that they are finely dispersed in small NPs.

As reported in Table 1, the specific surface area (SSA) of the FP-(X)Cu-T series was only slightly higher than that of the FSP-made pure TiO_2 (110 $m^2\ g^{-1}$), while the whole FP-(X)Cu/Pt-T series showed a somewhat higher SSA with respect to the other samples, with the FP-(0.05)Cu/Pt-T photocatalyst possessing the highest SSA, i.e., 153 $m^2\ g^{-1}$.

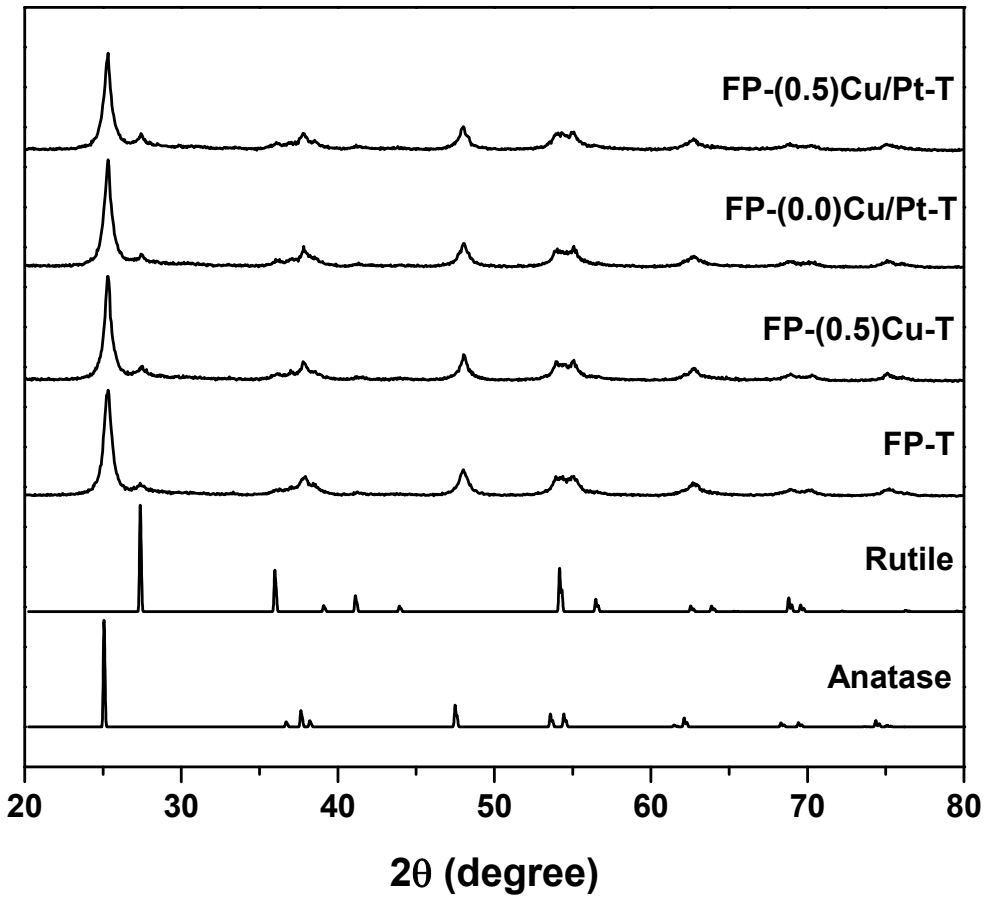

Figure 1. XRPD pattern of selected photocatalyst samples, with standard reference patterns of the anatase and rutile phases.

Table 1. Crystal phase composition, average anatase particles diameter d_A, and specific surface area SSA of the FSP-made photocatalysts.

Photocatalyst	Anatase (%)	Rutile (%)	d_A (nm)	SSA (m^2 g^{-1})
FP-T	88.6	11.4	13.9	110
FP-(0.05)Cu-T	83.2	16.8	13.8	116
FP-(0.1)Cu-T	91.8	8.2	14.3	119
FP-(0.5)Cu-T	78.9	21.1	17.1	115
FP-(0.0)Cu/Pt-T	87.3	12.7	14.0	131
FP-(0.05)Cu/Pt-T	91.9	8.1	12.8	153
FP-(0.1)Cu/Pt-T	87.7	12.3	13.4	130
FP-(0.2)Cu/Pt-T	82.4	17.6	14.9	127
FP-(0.3)Cu/Pt-T	83.5	16.5	14.9	129
FP-(0.5)Cu/Pt-T	82.0	18.0	15.2	121

2.1.2. UV-VIS Absorption Properties

The ultraviolet-visible (UV-VIS) absorption spectra of the FP-(X)Cu-T series together with that of bare FP-T are collected in Figure 2a. First of all, reference FP-T sample shows an important absorption tail in the whole visible light range originated from the carbonaceous impurities typical of FSP-made samples [26,28,29]. In the presence of copper the absorption of the materials increases, all FP-(X)Cu-T samples showing an extra absorption contribution in the 400–500 nm region, to be ascribed to the direct interfacial charge transfer (IFCT) of electrons from the VB of TiO_2 to Cu(II) surface species [12]. In addition, specific Cu(II) d-d transitions, evidenced by the absorption in the 700–800 nm region in

the spectrum of FP-(0.5)Cu-T (see Figure 2b), confirm that the here employed single-step FSP synthesis of Cu-containing TiO_2 stabilizes surface Cu_xO species, with copper in an oxidized state.

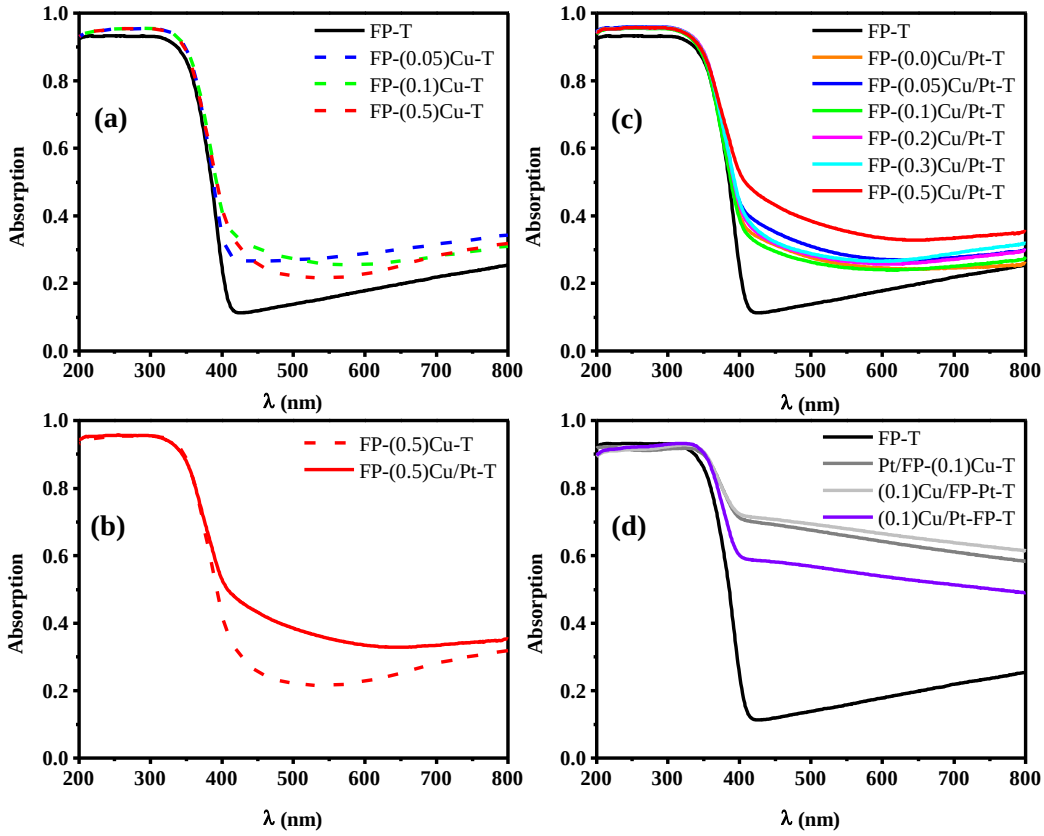

Figure 2. UV-VIS absorption spectra of (**a**) the FP-(X)Cu-T series; (**b**) FP-(0.5)Cu-T in comparison with FP-(0.5)Cu/Pt-T; (**c**) the FP-(X)Cu/Pt-T series and (**d**) the hybrid Pt and Cu co-modified TiO_2 samples prepared by combining FSP with Cu grafting and/or Pt NP deposition through the DP route.

All Pt-containing TiO_2 samples showed enhanced absorption with respect to the corresponding FP-(X)Cu-T photocatalysts (Figure 2c vs. Figure 2a), as clearly evidenced in Figure 2b, where the absorption spectrum of FP-(0.5)Cu/Pt-T is compared with that of FP-(0.5)Cu-T. However, the materials of the FP-(X)Cu/Pt-T series (characterized by a light grey color) showed a much lower absorption with respect to the Pt-Cu/TiO_2 "hybrid" samples prepared by combining the FSP technique with alternative TiO_2 surface modification routes implying post-deposition metal reduction (Figure 2c vs. Figure 2d). This indirectly confirms that, in FSP-made Pt/TiO_2 samples, platinum is also mostly present in oxidized, rather than in metallic, form [30] and that post-deposition chemical reduction may promote the reduction of both metal co-catalysts into metallic NPs (Figure 2d). Importantly, hybrid materials with identical co-catalyst content showed the same optical absorption profiles, independently of their preparation sequence (see Pt/FP-(0.1)Cu-T and (0.1)Cu/FP-Pt-T in Figure 2d). Compared to such materials, (0.1)Cu/Pt-FP-T, prepared by directly contacting the two metal precursors with the FP-T powder in subsequent steps, absorbs less light in the visible range and shows a UV-VIS absorption spectrum comparable to that of the photocatalyst obtained by applying exactly the same two-step deposition procedure to commercial P25 [22].

2.1.3. XPS Analysis

X-Ray photoelectron spectroscopy (XPS) analysis (see for example Figure 3 and Table 2) confirms the presence of ca. 20 at% of carbon in FSP-made materials. The C 1s signal exhibits a band peaking at

ca. 284.8 eV, which can be attributed to organic carbon, and a second peak at ca. 288 eV, ascribable to carbonaceous traces. The O 1s signal consists of a main peak at ca. 530.3 eV, originating from oxygen linked to titanium (Ti–O bonds) and a minor peak at ca. 532.5 eV compatible with oxygen in carbonate species, CO, CO_2, and in physisorbed water. The Ti 2p doublet signal is almost identical for all samples (Figure 3), with the main peak at ca. 458.8 eV and the second one at 464.5 eV, both typical of Ti^{4+} in TiO_2 [31]. The absence of shoulders at lower energy points to a negligible contribution of sub-stoichiometric titanium dioxide (TiO_{2-x}) or of Ti–OH surface groups [32–34]. This is also confirmed by the O/Ti ratio greater than 2 (Table 2). No signals originated from platinum and copper photoemission could be detected, their intensity possibly being below the detection limit.

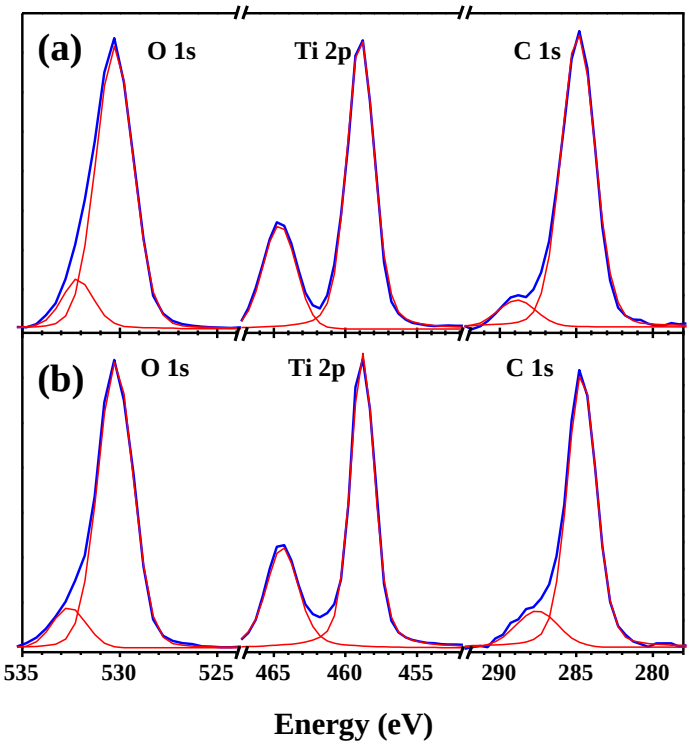

Figure 3. XPS spectra of the O 1s, Ti 2p, and C 1s regions for (**a**) FP-(0.0)Cu/Pt-T and (**b**) FP-(0.5)Cu/Pt-T.

Table 2. Results of the XPS analysis for 3 selected FP-(X)Cu/Pt-T photocatalysts.

Photocatalyst	Concentration (at%)			O/Ti Ratio
	O 1s	Ti 2p	C 1s	
FP-(0.0)Cu/Pt-T	55.4	23.5	19.7	2.36
FP-(0.05)Cu/Pt-T	54.6	23.1	21.0	2.36
FP-(0.5)Cu/Pt-T	53.5	22.2	23.4	2.41

2.1.4. HRTEM Analysis

Transmission electron microscopy (TEM) investigation of FP-(0.0)Cu/Pt-T (Figure 4a) and of FP-(0.5)Cu/Pt-T confirms the typical morphology of the flame made powder consisting of micro-aggregates of spherical nanocrystals. The TiO_2 particle size distribution obtained by counting 170 NPs (Figure 4b) is in the 4–28 nm range, with an average value of 11 nm and a standard deviation of 5 nm.

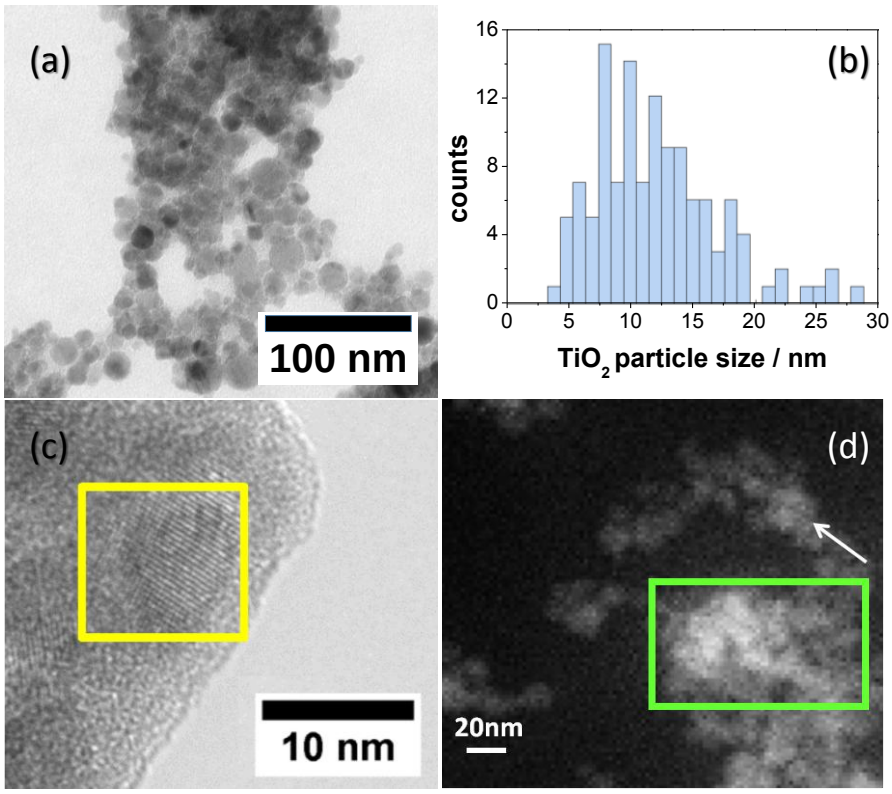

Figure 4. (**a**) TEM; (**b**) TiO_2 particle size distribution; (**c**) HRTEM; and (**d**) STEM-HAADF investigation of FP-(0.0)Cu/Pt-T. The green rectangle in (**d**) shows the acquisition area of the EDX spectrum. The white arrow points a surface Pt NP appearing as a bright dot due to the Z-contrast.

The high resolution TEM (HRTEM) image shown in Figure 4c confirms that the TiO_2 NPs are monocrystalline and that their crystal structure corresponds to the anatase phase. Indeed, the plane distance calculated by FFT analysis of the nanocrystals appearing within the yellow frame in Figure 4c is 3.5 Å, corresponding to the d-spacing of the [101] plane of anatase.

Pt NPs can be revealed by scanning transmission electron spectroscopy—high angular annular dark field (STEM-HAADF) analysis as bright dots on the TiO_2 surface because of its higher Z-contrast compared to the lighter Ti and O elements. However, Pt NPs can hardly be distinguished in Figure 4d (see for example the point indicated by the white arrow), in line with the fact that Pt is finely and homogeneously dispersed on the TiO_2 surface in the form of approximately 1 nm sized NPs. The presence of Pt was confirmed by energy dispersive X-ray spectroscopy (EDX) analysis, giving a 0.4 wt% of Pt for FP-(0.0)Cu/Pt-T, in good agreement with its nominal 0.5 wt% content. Similarly, EDX analysis of the FP-(0.5)Cu/Pt-T (dispersed on a molybdenum grid to avoid artefact on the Cu signal) confirmed the 0.5 wt% Cu content and its homogeneous dispersion on TiO_2.

2.2. *Photocatalytic Activity*

In the photocatalytic steam reforming of methanol the alcohol acts as an efficient hole scavenger, thus decreasing the electron-hole recombination rate and making conduction band electrons more readily available for H^+ reduction. Hydrogen production is, thus, coupled with methanol oxidation up to CO_2. Several intermediates, such as carbon monoxide, formic acid, or formaldehyde, are produced together with other side products, such as methane or ethane. H_2, CO_2, and CO accumulate at a constant rate in the closed recirculation system during the photocatalytic tests, according to pseudo-zero order kinetics.

The results obtained in methanol photosteam reforming photocatalytic tests are reported in Figure 5, in terms of hydrogen production rate, r_{H2}, and selectivity to CO_2 and CO, S_{CO2} and S_{CO}, as in previous studies [35]. We note, first of all, that the higher rate of hydrogen production r_{H2} obtained with FP-T with respect to P25 TiO_2 (3.6 vs. 2.7 mmol h^{-1} $g_{cat}{}^{-1}$) can be ascribed to the higher surface area and to the larger anatase content. On the other hand, these two reference samples behave in the same way regarding side-product formation, with similar selectivities towards carbon dioxide and monoxide (Figure 5). The r_{H2} values obtained with the photocatalysts of the FP-(X)Cu-T series were all around 7 mmol h^{-1} $g_{cat}{}^{-1}$, more than twice of those obtained with the bare materials, with a slightly decreasing rate with increasing copper loading. In addition to the beneficial effect on H_2 production rate, the presence of Cu species on the TiO_2 surface also influences the selectivity to CO in methanol photosteam reforming, the higher the amount of this metal, the lower being the selectivity to carbon monoxide. Thus, in the presence of copper as co-catalyst, preferential complete oxidation of methanol to carbon dioxide occurs, rather than to carbon monoxide, with a consequent higher rate of hydrogen production. In fact, full oxidation of one methanol molecule produces three H_2 molecules, while incomplete methanol oxidation to carbon monoxide produces two molecules of hydrogen per methanol molecule [35].

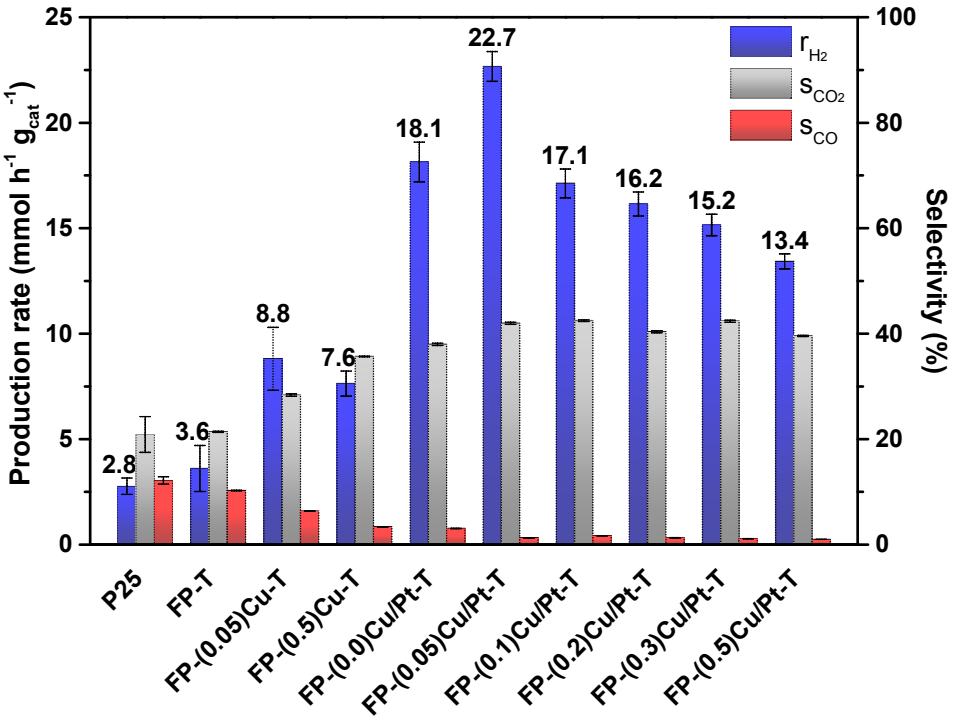

Figure 5. H_2 production rate (left ordinate) and selectivity to CO_2 and CO (right ordinate) obtained with Cu-containing TiO_2 and Cu/Pt-containing TiO_2 photocatalysts prepared by FSP in one step.

With respect to the Cu/TiO_2 photocatalysts obtained by grafting Cu on P25 TiO_2 [22] the photocatalysts of the FP-(X)Cu-T series showed a lower selectivity towards CO and a higher rate of hydrogen production. Considering two photocatalysts with the same 0.1 wt% Cu nominal content, the hydrogen production rate obtained with the FSP-made one is almost double (6.9 vs. 3.8 mmol h^{-1} $g_{cat}{}^{-1}$), with a halved selectivity to CO (6.1% vs. 10.8%). This might be a consequence of the formation of small NPs of crystalline copper oxides during the FSP synthesis, acting as semiconductors and thus forming a heterojunction with TiO_2, which improves the separation of the photoproduced charge couples [36]. In Cu/TiO_2 photocatalysts produced by the grafting technique the oxidized copper species on the TiO_2 surface are expected to be in amorphous form, as grafting is

carried out at room temperature and, thus, their action mechanism, consisting of switching between the Cu^{2+} and Cu^{+} oxidation states, may be different [12].

The presence of Pt on the FP-(X)Cu/Pt-T photocatalysts led to much higher photoactivity in terms of hydrogen production rate with respect to pure TiO_2 and to a ca. doubled photoactivity with respect to the FP-(X)Cu-T series. Platinum, due to its high work function (5.93 eV for the 111 crystal plane) [37], is a well-known, very efficient co-catalyst of TiO_2, particularly contributing to increased H^+ photocatalytic reduction leading to molecular hydrogen evolution [21,31,35,38,39]. As shown in Figure 5, the rate of photocatalytic hydrogen production obtained with the FSP-made Cu-Pt co-modified photocatalysts showed a bell-shaped trend, with the best performance in terms of r_{H2} (22.7 mmol h^{-1} $g_{cat}{}^{-1}$) being achieved with FP-(0.05)Cu/Pt-T, followed by the Pt-only containing sample FP-(0.0)Cu/Pt-T. Further increase of the copper content of the FSP-made photocatalysts had instead detrimental effects on the hydrogen production rate, with r_{H2} values lower than that obtained with copper-free FP-(0.0)Cu/Pt-T. The formation of an alloy between Cu and Pt during the FSP synthesis with the resulting decrease in the total work function of metal NPs and consequent decreased efficiency in H^+ reduction in comparison to pure platinum NPs, may be at the origin of such a behavior [35]. At the same time, the increase of nominal Cu content employed during the FSP synthesis may promote the formation of larger copper oxide domains, implying reduced Cu-TiO_2 interactions, which possibly determine a decrease of photocatalytic H_2 evolution [40].

Anyway, with increasing copper content in the FSP-made Cu-Pt/TiO_2 photocatalysts the selectivity towards carbon dioxide reached values up to 42% in the case of Cu- and Pt-containing photocatalysts, while the selectivity towards CO was significantly reduced. In fact, S_{CO} dropped from 3.1% and 3.4% for FP-(0.0)Cu/Pt-T and FP-(0.5)Cu-T, respectively, to 1.0% for FP-(0.5)Cu/Pt-T.

Concerning the photoactivity achieved by the "hybrid" samples, as shown in Figure 6, a limited increase in r_{H2} up to 10.6 mmol h^{-1} $g_{cat}{}^{-1}$ was attained upon platinum deposition by the DP method (see Pt/FP-(0.1)Cu-T vs. FP-(0.1)Cu-T), as a consequence of the above mentioned positive role played by platinum NPs in favoring electron-hole separation. On the other hand, Pt/FP-(0.1)Cu-T exhibits a photoactivity very similar to that obtained with (0.1)Cu/FP-Pt-T, in terms of both hydrogen production rate and selectivity to by-products. The obtained r_{H2} value is lower than that attained with the corresponding unmodified photocatalyst, i.e., FP-(0.0)Cu/Pt-T, and points to a negative effect of copper grafting on the photoactivity of Pt-containing FSP-made TiO_2. Surprisingly, (0.1)Cu/Pt-FP-T, obtained by Cu grafting followed by Pt deposition using the DP method on flame-made bare TiO_2, exhibits a hydrogen production rate much higher than that of the other two "hybrid" samples, containing the same nominal amount of metals.

Differently from the results obtained in our previous work on Cu-Pt modified TiO_2 photocatalysts prepared starting from commercial TiO_2 [22], with the presently investigated FSP-made Cu and Pt-containing TiO_2 photocatalysts no synergistic effect between the two metal co-catalysts was observed. In fact, with none of them a r_{H2} value was attained greater than the sum of those observed with the corresponding single metal (Pt or Cu)-modified TiO_2 photocatalyst. Nevertheless, a limited improvement in photoactivity was observed for very low copper content, i.e., in the case of FP-(0.05)Cu/Pt-T.

Thus, FSP proves to be an effective way to synthesize single metal-containing TiO_2-based photocatalysts, since both Cu-only and Pt-only containing FSP-made TiO_2 samples showed very high photoactivity in hydrogen production, performing better than TiO_2-based photocatalysts with analogous composition produced through wet-phase techniques, such as grafting of Cu or Pt deposition through the DP method.

Importantly, the beneficial effects induced in H_2 production by combining Cu(II) grafting with Pt NPs deposition on the TiO_2 surface by means of the DP procedure has been confirmed also in the case of bare FSP-made TiO_2, i.e., not only for commercial P25 [22]. In fact, though implying a more time-consuming procedure, the mild modification conditions ensured by these wet-phase techniques may avoid the undesired formation of a Cu-Pt alloy, with the consequent stabilization of

Cu nanoclusters, able to promote the transfer of photoexcited electrons from TiO_2 towards Pt NPs, where H_2 evolution occurs [22].

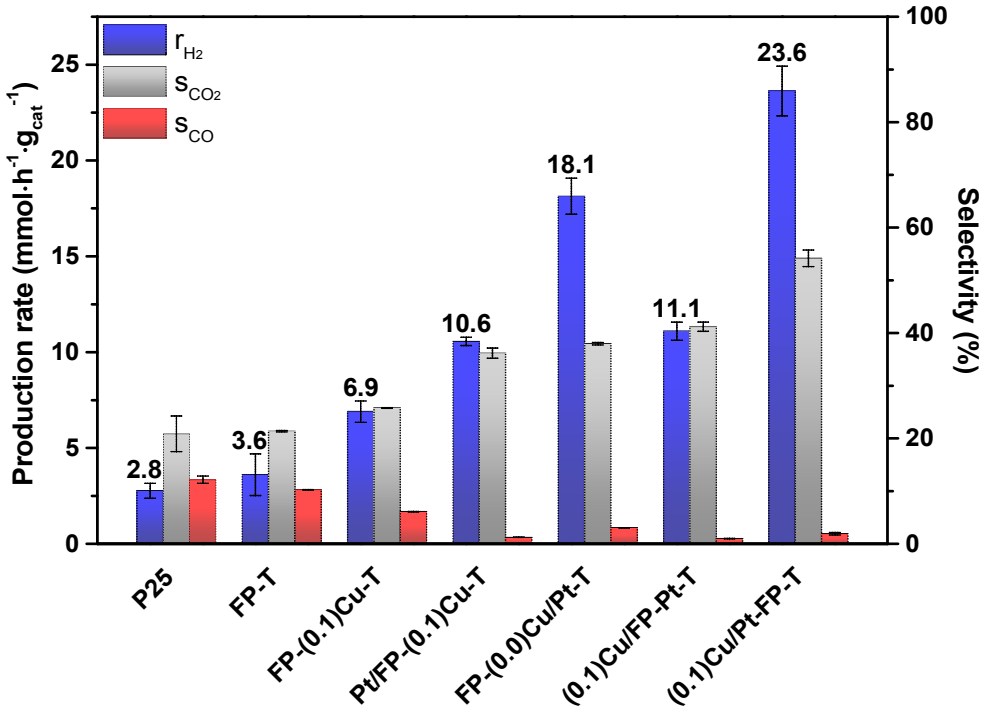

Figure 6. H_2 production rate (left ordinate) and selectivity to CO_2 and CO (right ordinate) obtained with photocatalysts prepared by combining different preparation techniques (see text).

3. Materials and Methods

3.1. Synthesis of the Photocatalysts

Except for commercial P25 TiO_2 from Degussa (Evonik, Essen, Germany), all investigated photocatalysts were home-prepared by FSP in a single step [41], employing a commercial FSP system (NPS10 Tethis S.p.A., Milano, Italy). The precursor solutions to be burned were prepared by mixing 25 mL of a 1.2 M titanium(IV)-tetraisopropoxide (TTIP) solution in xylene with a fixed volume (i.e., 5 mL) of a Pt-containing mother solution and/or variable volumes of a Cu-containing solution. This latter was prepared by dissolving 0.381 g of copper acetate monohydrate into 100 mL of propanoic acid. The Pt-containing mother solution was prepared by dissolving 0.135 g of hexachloroplatinic acid (30 wt% actual Pt content) into 50 mL of propanoic acid.

In order to maintain the combustion enthalpy constant in all synthesis, the xylene to propanoic acid volume ratio was, thus, kept constant (7:4) by diluting all solutions with 10 mL of xylene and with the required volume of propanoic acid, up to a 50 mL constant final volume.

The so-obtained solutions were injected into the burner at 4 mL min^{-1} by means of a syringe pump through a capillary tube and dispersed by pure oxygen (5.0 L min^{-1}). The spray was ignited by a methane/oxygen flamelet ring surrounding the nozzle. The methane and oxygen flow rates were 1.0 L min^{-1} and 2.0 L min^{-1}, respectively, and the pressure drop across the nozzle was kept constant at 2 bar. The powders were collected on glass fiber filters (Whatman, Maidstone, UK, model GF6, 257 mm in diameter) positioned 64 cm over the burner, on top of a steel vessel connected to a vacuum pump (Seco SV 1040C by Busch, Magden, Switzerland).

Two photocatalyst series were synthesized: the first series, labeled FP-(X)Cu-T, consisted of copper containing titanium dioxide powders; the second series, labeled FP-(X)Cu/Pt-T, consisted of platinum and copper containing powders. X corresponds to the Cu/Ti nominal weight percent ratio,

ranging from 0 to 0.5, while the Pt/Ti nominal weight percent ratio in the second series was fixed at 0.5. Bare titanium dioxide containing no Cu and Pt NPs was also produced by FSP and named FP-T.

Three additional samples were prepared by combining different metal NPs deposition techniques. Sample (0.1)Cu/Pt-FP-T was obtained from FP-T, by grafting 0.1 wt% of copper [42] and 0.5 wt% of platinum by the deposition-precipitation (DP) method [43], in two consecutive steps. Sample (0.1)Cu/FP-Pt-T was obtained by grafting Cu on the surface of FP-(0.0)Cu/Pt-T, followed by the addition of an aqueous $NaBH_4$ solution in slight excess. Sample Pt-FP-(0.1)Cu-T was obtained by DP of Pt NPs on FP-(0.1)Cu-T. Briefly, the grafting method [42] consists in drying under vigorous stirring and heating at 90 °C an aqueous suspension containing ($Cu(NO_3)_2 \cdot 3H_2O$) and the dispersed TiO_2 powder. The DP technique [43] consists of stirring a heated aqueous suspension containing the starting photocatalyst and H_2PtCl_6 in the presence of urea to induce the precipitation of Pt NPs, followed by reduction of the so obtained powder with $NaBH_4$ in an aqueous dispersion.

All chemicals were purchased from Sigma-Aldrich (St. Louis, MO, USA) and used as received.

3.2. Characterization of the Photocatalysts

XRPD analyses were performed using a Philips PW3020 powder diffractometer (PANalytical, Almelo, The Netherlands), operating at 40 kV and 40 mA and exploiting copper Kα radiation (λ = 1.54056 Å) as X-ray source. The diffractograms were recorded by scanning between 5° and 80° 2θ angles, with a 0.05° step. Phase quantitative analysis was made by the Rietveld refinement method [44], using Quanto software (Ver. 1.0, free licence software) [45]; the mean anatase crystallite size was calculated by applying the Scherrer equation [46], from the width of the most intense reflection at 2θ = 25.4°.

The BET specific surface area (SSA) was measured by N_2 adsorption/desorption at liquid nitrogen temperature in a Micromeritics ASAP 2010 (Micromeritics, Norcross, GA, USA) apparatus after out-gassing in vacuo at 150 °C for 2 h. UV-VIS diffuse reflectance (R) analysis was performed with a Jasco V-670 spectrophotometer (Jasco, Easton, MD, USA) equipped with a PIN-757 integrating sphere, using barium sulfate as a reference. The results are presented as absorption (A) spectra (A = 1 − R).

XPS data were collected by a PHI-5500 Physical Electronics spectrometer (Physical Electronics, Chanhassen, MN, USA) equipped with an aluminum anode (Kα = 1486.6 eV) as the monochromatized source, operating at 200 W applied power, with a 58.7 eV pass energy, 0.5 eV energy step, and a 0.15 s step time. The vacuum level during the analyses was ca. 10^{-9} Torr and a neutralizer was used in order to avoid surface electrostatic charge accumulation on the nonconductive samples.

HRTEM analysis was carried out with a Zeiss LIBRA 200FE transmission electron microscope (Zeiss, Oberkochen, Germany), equipped with STEM—HAADF and EDX (Oxford X-Stream 2 and INCA software). The microscope has a 200 kV field emission gun-like source with an in-column second-generation omega filter for energy-selective spectroscopy. The sample was dispersed in isopropanol and then a drop of the suspension was deposited on a 300 mesh holey carbon copper or molybdenum grid.

3.3. Photocatalytic Tests

The photocatalytic activity in hydrogen production from methanol photo-steam reforming was tested in the already described stainless steel closed system [5], which was modified by substituting the Plexiglas photoreactor with a new stainless-steel photoreactor, with a front round hollow (4 mm thick and 63.5 mm in diameter), closed by a Pyrex glass window. The temperature of this new cell can be increased by means of four heating cartridges regulated by a thermocouple. The photocatalytic bed, placed in the front hollow of the photoreactor, was prepared by mixing 15 ± 2 mg of photocatalyst and 7.10 ± 0.05 g of 20–40 mesh (0.42–0.85 mm) quartz beads with few droplets of distilled water, followed by drying in an oven at 70 °C. Prior to any run, the whole system was purged in the dark with pure nitrogen at 110 mL min^{-1} for 40 min in order to remove any trace of oxygen. The temperature of the photoreactor was fixed at 40 °C and set at this value 30 min before the beginning of the experiment,

with a heating rate of 10 °C min^{-1}. Then the gas phase, saturated with methanol and water vapors by bubbling nitrogen into a 20 vol% methanol aqueous solution kept at 30 °C, was continuously recirculated at a constant rate (60 mL min^{-1}) by means of a bellow pump for 15 min before starting the test. During the photocatalytic run, the gas flow was also set at 60 mL min^{-1}. The absolute pressure inside the system, initially 1.2 bar, gradually increased during the run due to the accumulation of gas products. The light source, always switched on 30 min before the beginning of the run and placed at ca. 20 cm from the photoreactor, was a 300 W xenon arc lamp (LSH302, LOT-Oriel, Darmstadt, Germany), emitting in the 350–400 nm range. The light intensity on the photocatalyst was 0.31 W cm^{-2}, as measured with an optical power meter (model PM200 by Thorlabs, Newton, NJ, USA) equipped with a thermal power sensor (Thorlabs S302C).

The gas-phase composition was analyzed on-line during irradiation by means of a gas chromatograph (GC, Agilent 6890N, by Agilent, Santa Clara, CA, USA) equipped with two capillary columns (HP-PlotU and Molesieve 5A), two detectors (thermo conductivity and flame ionization) and a Ni-catalyst system for CO_2 and CO methanation. The instrument was preliminary calibrated for H_2, CO_2, CO, CH_4, and H_2CO analyses. The amount of formic acid produced during the photoreaction and accumulated in the aqueous solution was determined by ion chromatography at the end of the run, employing a Metrohm 761 Compact IC instrument (by Metrohm AG, Herisau, Switzerland), equipped with an anionic Metrosep A column.

The results of photocatalytic tests are reported as H_2 production rate (r_{H2}), obtained as the slope of the straight lines of the produced hydrogen amount (normalized per unit catalyst weight) vs. the irradiation time plots. The selectivity in hydrogen production was calculated from the rates of CO_2 and CO formation (r_{CO2} and r_{CO}), as the ratio between these latter and the rate of H_2 production from methanol, by taking into account the stoichiometry of the CO_2 and CO formation reactions [35].

$$CH_3OH + H_2O \overset{hv,TiO_2}{\rightarrow} 3H_2 + CO_2$$

$$CH_3OH \overset{hv,TiO_2}{\rightarrow} 2H_2 + CO$$

$$S_{CO_2} = \frac{3r_{co_2}}{r_{H_2}}$$

$$S_{CO} = \frac{2r_{CO}}{r_{H_2}}$$

To ensure the reproducibility of the data, the photocatalytic tests were repeated at least twice with each sample, using the same photocatalytic bed; at the end of each run, the water/methanol solution in the flask was changed and the whole system was purged with N_2 in the dark for 30 min prior to start a new run.

4. Conclusions

In conclusion, FSP proves to be an effective way to synthesize highly-performing single metal-containing TiO_2-based photocatalysts for photocatalytic hydrogen production. However, the highest synergistic effect between the Cu and Pt co-catalysts was attained with photocatalysts prepared by wet-phase methods on bare FSP-made TiO_2, i.e., Cu(II) grafting followed by Pt NP deposition.

Copper overloading (up to 0.5 wt%) of FSP-made photocatalysts is detrimental for H_2 production rate, probably due to Cu-Pt alloying under the here employed harsh synthesis conditions. Nevertheless, the addition of very low amounts of copper (0.05 wt%) during the FSP synthesis of Pt/TiO_2 guarantees a ca. 20% improvement of the overall photocatalytic hydrogen production, together with a lower selectivity towards the less desired carbon monoxide side-product.

Acknowledgments: The collaboration of Laura Meda, Istituto ENI Donegani, Novara, in XPS analysis is gratefully acknowledged. This work received financial support from the Italian MIUR, through the PRIN 2015 SMARTNESS

(2015K7FZLH) project. The use of instrumentation purchased through the Regione Lombardia—Fondazione Cariplo joint SmartMatLab project (Fondazione Cariplo 2013-1766 project) is gratefully acknowledged.

Author Contributions: G.L.C., M.V.D., and E.S. conceived and designed the experiments and contributed in writing the manuscript; M.B. performed all experiments and data analyses, wrote a draft of the paper, and contributed to its revision; L.G.B. contributed to the FSP synthesis of the materials; A.M.F. performed and interpreted electron microscopy analyses; and M.V.D. and E.S. provided the final revision of the manuscript.

Conflicts of Interest: The authors declare no conflict of interest.

References

1. Cherry, R.S. A hydrogen utopia? *Int. J. Hydrogen Energy* **2004**, *29*, 125–129. [CrossRef]
2. Chaubey, R.; Sahu, S.; James, O.O.; Maity, S. A review on development of industrial processes and emerging techniques for production of hydrogen from renewable and sustainable sources. *Renew. Sustain. Energy Rev.* **2013**, *23*, 443–462. [CrossRef]
3. Rahimi, N.; Pax, R.A.; Gray, E.M.A. Review of functional titanium oxides. I: TiO_2 and its modifications. *Prog. Solid State Chem.* **2016**, *44*, 86–105. [CrossRef]
4. Ma, Y.; Wang, X.L.; Jia, Y.S.; Chen, X.B.; Han, H.X.; Li, C. Titanium Dioxide-Based Nanomaterials for Photocatalytic Fuel Generations. *Chem. Rev.* **2014**, *114*, 9987–10043. [CrossRef] [PubMed]
5. Chiarello, G.L.; Forni, L.; Selli, E. Photocatalytic hydrogen production by liquid- and gas-phase reforming of CH_3OH over flame-made TiO_2 and Au/TiO_2. *Catal. Today* **2009**, *144*, 69–74. [CrossRef]
6. Gomathisankar, P.; Noda, T.; Katsumata, H.; Suzuki, T.; Kaneco, S. Enhanced hydrogen production from aqueous methanol solution using TiO_2/Cu as photocatalysts. *Front. Chem. Sci. Eng.* **2014**, *8*, 197–202. [CrossRef]
7. Pérez-Larios, A.; Hernández-Gordillo, A.; Morales-Mendoza, G.; Lartundo-Rojas, L.; Mantilla, A.; Gomez, R. Enhancing the H_2 evolution from water-methanol solution using Mn^{2+}-Mn^{+3}-Mn^{4+} redox species of Mn-doped TiO_2 sol-gel photocatalysts. *Catal. Today* **2016**, *266*, 9–16. [CrossRef]
8. Wang, Q.; An, N.; Bai, Y.; Hang, H.; Li, J.; Lu, X.; Liu, Y.; Wang, F.; Li, Z.; Lei, Z. High photocatalytic hydrogen production from methanol aqueous solution using the photocatalysts CuS/TiO_2. *Int. J. Hydrogen Energy* **2013**, *38*, 10739–10745. [CrossRef]
9. Kawai, T.; Sakata, T. Conversion of carbohydrate into hydrogen fuel by a photocatalytic process. *Nature* **1980**, *286*, 474–476. [CrossRef]
10. Choi, H.J.; Kang, M. Hydrogen production from methanol/water decomposition in a liquid photosystem using the anatase structure of Cu loaded TiO_2. *Int. J. Hydrogen Energy* **2007**, *32*, 3841–3848. [CrossRef]
11. Chiarello, G.L.; Dozzi, M.V.; Selli, E. TiO_2-based materials for photocatalytic hydrogen production. *J. Energy Chem.* **2017**, *26*, 250–258. [CrossRef]
12. Irie, H.; Kamiya, K.; Shibanuma, T.; Miura, S.; Tryk, D.A.; Yokoyama, T.; Hashimoto, K. Visible light-sensitive Cu(II)-grafted TiO_2 photocatalysts: Activities and X-ray absorption fine structure analyses. *J. Phys. Chem. C* **2009**, *113*, 10761–10766. [CrossRef]
13. Liu, Y.; Wang, Z.; Huang, W. Influences of TiO_2 phase structures on the structures and photocatalytic hydrogen production of CuO_x/TiO_2 photocatalysts. *Appl. Surf. Sci.* **2016**, *389*, 760–767. [CrossRef]
14. Luna, A.L.; Novoseltceva, E.; Louarn, E.; Beaunier, P.; Kowalska, E.; Ohtani, B.; Valenzuela, M.A.; Remita, H.; Colbeau-Justin, C. Synergetic effect of Ni and Au nanoparticles synthesized on titania particles for efficient photocatalytic hydrogen production. *Appl. Catal. B Environ.* **2016**, *191*, 18–28. [CrossRef]
15. Barrios, C.E.; Albiter, E.; Gracia y Jimenez, J.M.; Tiznado, H.; Romo-Herrera, J.; Zanella, R. Photocatalytic hydrogen production over titania modified by gold—Metal (palladium, nickel and cobalt) catalysts. *Int. J. Hydrogen Energy* **2016**, *41*, 1–14. [CrossRef]
16. Kotesh Kumar, M.; Bhavani, K.; Naresh, G.; Srinivas, B.; Venugopal, A. Plasmonic resonance nature of Ag-Cu/TiO_2 photocatalyst under solar and artificial light: Synthesis, characterization and evaluation of H_2O splitting activity. *Appl. Catal. B Environ.* **2016**, *199*, 282–291. [CrossRef]

17. Nischk, M.; Mazierski, P.; Wei, Z.; Siuzdak, K.; Kouame, N.A.; Kowalska, E.; Remita, H.; Zaleska-Medynska, A. Enhanced photocatalytic, electrochemical and photoelectrochemical properties of TiO_2 nanotubes arrays modified with Cu, AgCu and Bi nanoparticles obtained via radiolytic reduction. *Appl. Surf. Sci.* **2016**, *387*, 89–102. [CrossRef] [PubMed]
18. Janczarek, M.; Wei, Z.; Endo, M.; Ohtani, B.; Kowalska, E. Silver-and copper-modified decahedral anatase titania particles as visible light-responsive plasmonic photocatalyst. *J. Photonics Energy* **2017**, *7*, 12008. [CrossRef]
19. Shiraishi, Y.; Sakamoto, H.; Sugano, Y.; Ichikawa, S.; Hirai, T. Pt-Cu bimetallic alloy nanoparticles supported on anatase TiO_2: Highly active catalysts for aerobic oxidation driven by visible light. *ACS Nano* **2013**, *7*, 9287–9297. [CrossRef] [PubMed]
20. Teng, F.; Chen, M.; Li, N.; Hua, X.; Wang, K.; Xu, T. Effect of TiO_2 Surface Structure on the Hydrogen Production Activity of the Pt@CuO/TiO_2 Photocatalysts for Water Splitting. *ChemCatChem* **2014**, *6*, 842–847. [CrossRef]
21. Jung, M.; Hart, J.N.; Boensch, D.; Scott, J.; Ng, Y.H.; Amal, R. Hydrogen evolution via glycerol photoreforming over Cu-Pt nanoalloys on TiO_2. *Appl. Catal. A Gen.* **2016**, *518*, 221–230. [CrossRef]
22. Dozzi, M.V.; Chiarello, G.L.; Pedroni, M.; Livraghi, S.; Giamello, E.; Selli, E. High Photocatalytic Hydrogen Production on Cu(II) Pre-grafted Pt/TiO_2. *Appl. Catal. B Environ.* **2017**, *209*, 417–428. [CrossRef]
23. Teoh, W.Y.; Mädler, L.; Beydoun, D.; Pratsinis, S.E.; Amal, R. Direct (one-step) synthesis of TiO_2 and Pt/TiO_2 nanoparticles for photocatalytic mineralisation of sucrose. *Chem. Eng. Sci.* **2005**, *60*, 5852–5861. [CrossRef]
24. Strobel, R.; Baiker, A.; Pratsinis, S.E. Aerosol flame synthesis of catalysts. *Adv. Powder Technol.* **2006**, *17*, 457–480. [CrossRef]
25. Pratsinis, S.E.; Vemury, S. Particle formation in gases: A review. *POWDER Technol.* **1996**, *88*, 267–273. [CrossRef]
26. Chiarello, G.L.; Selli, E.; Forni, L. Photocatalytic hydrogen production over flame spray pyrolysis-synthesised TiO_2 and Au/TiO_2. *Appl. Catal. B Environ.* **2008**, *84*, 332–339. [CrossRef]
27. Teleki, A.; Bjelobrk, N.; Pratsinis, S.E. Flame-made Nb- and Cu-doped TiO_2 sensors for CO and ethanol. *Sens. Actuators B Chem.* **2008**, *130*, 449–457. [CrossRef]
28. Chiarello, G.L.; Rossetti, I.; Lopinto, P.; Migliavacca, G.; Forni, L. Preparation by flame spray pyrolysis of $ABO_{3\pm\delta}$ catalysts for the flameless combustion of methane. *Catal. Today* **2006**, *117*, 549–553. [CrossRef]
29. Chiarello, G.L.; Rossetti, I.; Forni, L.; Lopinto, P.; Migliavacca, G. Solvent nature effect in preparation of perovskites by flame pyrolysis. 2. Alcohols and alcohols + propionic acid mixtures. *Appl. Catal. B Environ.* **2007**, *72*, 227–232. [CrossRef]
30. Chiarello, G.L.; Dozzi, M.V.; Scavini, M.; Grunwaldt, J.-D.; Selli, E. One step flame-made fluorinated Pt/TiO_2 photocatalysts for hydrogen production. *Appl. Catal. B Environ.* **2014**, *160–161*, 144–151. [CrossRef]
31. Dozzi, M.V.; Zuliani, A.; Grigioni, I.; Chiarello, G.L.; Meda, L.; Selli, E. Photocatalytic activity of one step flame-made fluorine doped TiO_2. *Appl. Catal. A Gen.* **2016**, *521*, 220–226. [CrossRef]
32. Reyes-Garcia, E.A.; Sun, Y.; Reyes-Gil, K.R.; Raftery, D. Solid-state NMR and EPR analysis of carbon-doped titanium dioxide photocatalysts ($TiO_{2-x}C_x$). *Solid State Nucl. Magn. Reson.* **2009**, *35*, 74–81. [CrossRef] [PubMed]
33. Yang, J.; Bai, H.; Tan, X.; Lian, J. IR and XPS investigation of visible-light photocatalysis-Nitrogen-carbon-doped TiO_2 film. *Appl. Surf. Sci.* **2006**, *253*, 1988–1994. [CrossRef]
34. Caruso, T.; Lenardi, C.; Agostino, R.G.; Amati, M.; Bongiorno, G.; Mazza, T.; Policicchio, A.; Formoso, V.; Maccallini, E.; Colavita, E.; et al. Electronic structure of cluster assembled nanostructured TiO_2 by resonant photoemission at the Ti $L_{2,3}$ edge. *J. Chem. Phys.* **2008**, *128*, 94704. [CrossRef] [PubMed]
35. Chiarello, G.L.; Aguirre, M.H.; Selli, E. Hydrogen production by photocatalytic steam reforming of methanol on noble metal-modified TiO_2. *J. Catal.* **2010**, *273*, 182–190. [CrossRef]
36. DeMeo, D.; MacNaughton, S.; Sonkusale, S.; Vandervelde, T. Electrodeposited Copper Oxide and Zinc Oxide Core-Shell Nanowire Photovoltaic Cells. In *Nanowires—Implementations and Applications*; Hashim, A., Ed.; InTech: Rijeka, Croatia, 2011; pp. 141–156, ISBN 978-953-307-318-7.
37. Lide, D.R.R.; Haynes, W.M.M.; Baysinger, G.; Berger, L.I.; Roth, D.L.; Zwillinger, D.; Frenkel, M.; Goldberg, R.N. *CRC Handbook of Chemistry and Physics*; Internet, V., Ed.; CRC Press: Boca Raton, FL, USA, 2005.
38. Vorontsov, A.V.; Dubovitskaya, V.P. Selectivity of photocatalytic oxidation of gaseous ethanol over pure and modified TiO_2. *J. Catal.* **2004**, *221*, 102–109. [CrossRef]

39. Chiarello, G.L.; Paola, D.; Selli, E. Effect of titanium dioxide crystalline structure on the photocatalytic production of hydrogen. *Photochem. Photobiol. Sci.* **2011**, *10*, 355–360. [CrossRef] [PubMed]
40. Jung, M.; Scott, J.; Ng, Y.H.; Jiang, Y.; Amal, R. CuO_x dispersion and reducibility on TiO_2 and its impact on photocatalytic hydrogen evolution. *Int. J. Hydrogen Energy* **2014**, *39*, 12499–12506. [CrossRef]
41. Chiarello, G.L.; Rossetti, I.; Forni, L. Flame-spray pyrolysis preparation of perovskites for methane catalytic combustion. *J. Catal.* **2005**, *236*, 251–261. [CrossRef]
42. Morikawa, T.; Irokawa, Y.; Ohwaki, T. Enhanced photocatalytic activity of $TiO_{2-x}N_x$ loaded with copper ions under visible light irradiation. *Appl. Catal. A Gen.* **2006**, *314*, 123–127. [CrossRef]
43. Dozzi, M.V.; Prati, L.; Canton, P.; Selli, E. Effects of gold nanoparticles deposition on the photocatalytic activity of titanium dioxide under visible light. *Phys. Chem. Chem. Phys.* **2009**, *11*, 7171–7180. [CrossRef] [PubMed]
44. Rietveld, H.M. A profile refinement method for nuclear and magnetic structures. *J. Appl. Crystallogr.* **1969**, *2*, 65–71. [CrossRef]
45. Altomare, A.; Burla, M.C.; Giacovazzo, C.; Guagliardi, A.; Moliterni, A.G.G.; Polidori, G.; Rizzi, R. Quanto: A Rietveld program for quantitative phase analysis of polycrystalline mixtures. *J. Appl. Crystallogr.* **2001**, *34*, 392–397. [CrossRef]
46. Scherrer, P. Estimation of the size and internal structure of colloidal particles by means of Röntgen rays. *Göttinger Nachrichten Math. Phys.* **1918**, *2*, 98–100.